Coupled Heat and Mass Transfer Processes in Enclosed Environments

Ravindra Dwivedi[1] and John L. Wilson[*,2]
[1,2]New Mexico Institute of Mining and Technology
*Corresponding author: MSEC 242, Dept of Earth & Environmental Science
New Mexico Institute of Mining and Technology
801 Leroy Place, Socorro, NM 87801, jwilson@nmt.edu

Abstract: Geothermally driven natural convection in enclosures is a ubiquitous process occurring in many physical environments such as caves, mines, etc.

We have numerically simulated laminar and turbulent natural convection in isolated air-filled cavities, buried in a more (in comparison to the air-filled cavity) conductive rock mass. To better understand the convective heat transfer process in isolated cavities, we varied the parameters of aspect ratio, slope, and the geometry of a cavity. To characterize the numerical results, we used metrics including Nusselt (*Nu*) vs. Rayleigh (*Ra*) number behavior as well as the number and pattern of convection cells.

Keywords: cavity, heat transfer, laminar, turbulent, convection

1. Introduction

Natural convection is ubiquitous in various geophysical scenarios (e.g., air or water-filled fractures in rocks situated in geothermal zones, very deep mines, naturally occurring cavities, and in human-made excavations), especially those excavations and cavities in a geothermal resource area. Natural convection also has multitudinous applications; for example, natural cooling of electronic components in the Central Processing Unit of a computer system, cooling of a nuclear reactor, and the natural ventilation of environmental friendly, cost efficient homes. Given the ubiquity of the convection process, there is much literature regarding theoretical [15], experimental ([11], [9], [2], [16]) and numerical modeling work ([3], [5], [10]) on natural convection in enclosures. A concise and current description of the theory as well as experimental and numerical work can be found in [4]. Alternatively, other researchers considered convection in saturated porous media; a review can be found in [17]. However, we are interested in air-filled enclosures only. In contrast to the voluminous amount of research on isolated enclosures with various combinations of boundary conditions (see [14] and [1]), there is very little research on air-filled enclosures buried in a more conductive rock mass. Some research on the subject is aimed to a very specific field, namely, cave micrometeorology [18].

Our goal is to understand non-linear and coupled heat transport and fluid flow processes in enclosures completely buried in a more conductive rock mass, as compared to the air-filled enclosure. We used a realistic value of geothermal heat flux at the rock mass bottom boundary. We consider the following cases: a cavity with various aspect ratios A (e.g., 0.5, 2, 10, and infinity [see Figure 1a]), a cavity with various slopes from the horizontal line (see Figure 1b), and a cavity with various geometries (see Figure 2).

Section 2 briefly describes the use of the COMSOL Multiphysics software package, and the governing equations along with boundary conditions, section 3 describes results and discussion, and section 4 presents conclusions based on the presented results.

2 Use of COMSOL Multiphysics and Governing Equations

Geothermally driven natural convection is caused by the strong coupling of the heat transfer processes and fluid flow. Heat transfer occurs throughout the rock mass (conduction only) and cavity (conduction and convection), while flow is restricted to the cavity.

We have modeled heat transfer using COMSOL's Convection and Conduction mode. We used the Navier-Stokes mode for momentum transport in the laminar flow simulations and the k-ω turbulence model in turbulent flow simulations.

Note: For interpretation of various symbols used in this paper, please refer to Table 3 in the Appendix.

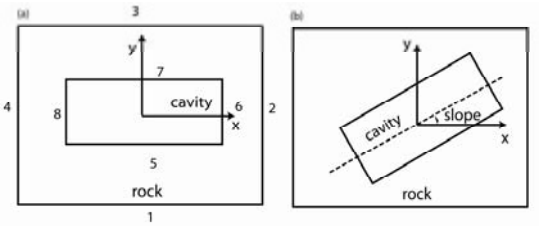

Figure 1: (a) Schematic diagram for the cavity aspect ratio case (Note: For an infinitely wide cavity boundaries 5 and 7 extend to boundaries 2 and 4; distance between any cavity boundary to corresponding rock boundary is 5*A*); (b) Schematic diagram for the cavity slope case

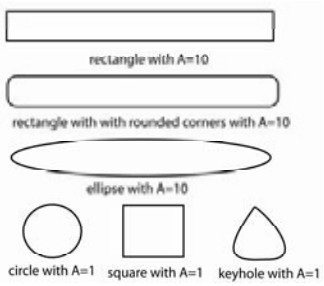

Figure 2: Schematic diagram for the cavity geometry case

2.1 **Governing Equations and Boundary Conditions**

Fluid mechanists prefer to use governing equations in a non-dimensional form because it helps locate the essential parameters for coupled flow and heat transport problems, and it is easier to study the gradual impact of the driving mechanism or forcing on the flow and heat transport system. Consistent with these objectives, we have developed two sets of governing equations using two different sets of characteristic scales for length, fluid speed, and temperature.

2.1.1 Model # 1: For Low *Ra* Convection

In this model, the following characteristic scales are used in non-dimensionalizing the governing equations for flow and heat transport: length scale H, velocity scale (λ /H), temperature scale $T = (T_1\text{-}T)/(T_1\text{-}T_2)$.

Conservation of mass:

$$\nabla \cdot \vec{u} = 0 \tag{1}$$

Conservation of momentum:

$$\vec{u} \cdot \nabla \vec{u} = -\nabla P + (Pr + F_{lt}\mu_T)\nabla^2 \vec{u} + (RaPrT)\,\vec{j} \tag{2}$$

Transport of k:

$$F_{lt}(\vec{u} \cdot \nabla k = \nabla \cdot [(Pr + \sigma_k \mu_T)\nabla k] + \frac{\mu_T (\nabla \vec{u})^2}{2} - \beta_k k\omega) \tag{3}$$

Transport of ω:

$$F_{lt}(\vec{u} \cdot \nabla \omega = \nabla \cdot [(Pr + \sigma_\omega \mu_T)\nabla \omega] + \frac{a\omega\mu_T (\nabla \vec{u})^2}{2k} - \beta\omega^2) \tag{4}$$

Conservation of energy:

$$\frac{K_f}{K_r}\vec{u} \cdot \nabla T = \frac{QH^2}{K_f \Delta T} + \nabla \cdot [(\frac{K_f}{K_r} + F_{lt}K_T)\nabla T] \tag{5}$$

Eddy Viscosity:

$$\mu_T = \frac{k}{\omega} \tag{6}$$

Turbulent thermal conductivity:

$$K_T = \frac{\mu_T}{Pr_T}(\frac{K_f}{K_r}) \tag{7}$$

2.1.2 Model # 2: For high *Ra* convection

In this model, the following characteristic scales are used in non-dimensionalizing the governing equations for flow and heat transport: length scale H, velocity scale $(\lambda/H)Ra^{0.5}$, temperature scale $T = (T_1\text{-}T)/(T_1\text{-}T_2)$.

Conservation of mass:

$$\nabla \cdot \vec{u} = 0 \tag{8}$$

Conservation of momentum:

$$\vec{u} \cdot \nabla \vec{u} = -\nabla P + (\frac{Pr}{\sqrt{Ra}}\frac{K_f}{K_r} + F_{lt}\mu_T)\nabla^2 \vec{u} + (PrT(\frac{K_f}{K_r})^2)\,\vec{j} \tag{9}$$

Transport of k:

$$F_{lt}(\vec{u} \cdot \nabla k = \nabla \cdot [(\frac{Pr}{\sqrt{Ra}}\frac{K_f}{K_r} + \sigma_k \mu_T)\nabla k] + \frac{\mu_T (\nabla \vec{u})^2}{2} - \beta_k k\omega) \tag{10}$$

Transport of ω:

$$F_{lt}(\vec{u} \cdot \nabla \omega = \nabla \cdot [(\frac{Pr}{\sqrt{Ra}}\frac{K_f}{K_r} + \sigma_\omega \mu_T)\nabla \omega] + \frac{a\omega\mu_T (\nabla \vec{u})^2}{2k} - \beta\omega^2) \tag{11}$$

Conservation of energy:

$$\sqrt{Ra}\vec{u} \cdot \nabla T = \frac{QH^2}{K_f \Delta T} + \nabla \cdot [(\frac{K_f}{K_r} + F_{lt}K_T)\nabla T] \tag{12}$$

Eddy Viscosity:

$$\mu_T = \frac{k}{\omega} \tag{13}$$

Turbulent thermal conductivity:

$$K_T = \frac{\mu_T \sqrt{Ra}}{Pr_T} \tag{14}$$

Two separate models of governing equations are required. Model #1 is effective for laminar convection simulation in small enclosures and, as in comparison to model # 2, it is more

intuitive. When Ra is 0, there is no forcing in the momentum balance equation, thus mimicking conductive heat transfer in a cavity. Whereas, when Ra is higher than some threshold, there is both conductive and convective heat transfer in a cavity. When the model # 1 is used for either laminar convection in enclosures with a high aspect ratio or for turbulent convection, the model yielded a convergence problem. Model #2 is effective for this case and helps achieve a converged result. However, we cannot use model # 2 when Ra is 0, because the fluid viscosity term in the momentum balance equation in not defined for Ra equals to 0.

It is clear from these two models that in a non-dimensional form, there are only two independent parameters, *Ra* and *Pr*, and if geometry or the computational domain is also considered as an independent parameter, then there are three independent parameters, namely, *Ra*, *Pr*, and *A*. Additionally, we have employed Boussinesq approximation [7] in simplifying the governing equations. Refer to [6] for more details on the derivation of the governing equations in a non-dimensional form.

2.1.3 Boundary conditions:

Table 1 shows boundary conditions used in simulation of laminar and turbulent natural convection. Additionally, for an infinitely wide cavity, periodic boundary condition for *u, v, p, T* are used. Figure 3 shows a typical mesh discretization used in the simulations.

3. Results and Discussion

Part 1:

The presence of a cavity affects the heat flux flow pattern in the surrounding rock mass. This effect is caused by the insulation effect of the air-filled cavity. The effect is more pronounced as a cavity aspect ratio (*A*), which is defined as a cavity width to height ratio, increases. Wider air-filled cavities (large *A*) have large insulation effects relative to smaller cavities (small *A*), because heat flux has to travel a longer distance and go around the cavity. However, for a given aspect ratio, when buoyancy forcing, that is *Ra* is increased, more heat flux passes through the cavity. This is indicated by the reduction in the curvature of temperature contours around the cavity (see Figure 4 a, b, and c). When fluid flow behavior is turbulent in nature, temperature contours in the proximity of the cavity are almost horizontal (see Figure 4c), thus indicating heat flux will pass through the cavity rather than avoid it.

Table (1): Boundary conditions used for laminar and turbulent natural convection simulations (Note: Boundary numbers refer to boundaries show in figure 1a)

Boundary #	Flow type			
	Laminar flow		Turbulent flow	
	Heat	Fluid	Heat	Fluid
1	q=1	[-]	q=1	[-]
2,4	q=0	[-]	q=0	[-]
3	T=0	[-]	T=0	[-]
5,6,7,8	continuity	no-slip	continuity	no-slip, k=0, ω=Pr/h^2

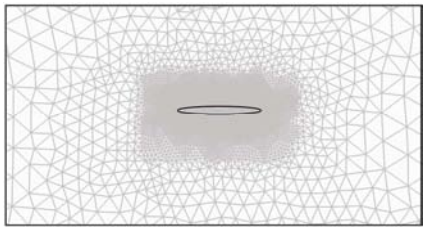

Figure 3: A close-up view of a typical mesh discretization used in the simulations (Note: geometry in black shows an elliptical cavity)

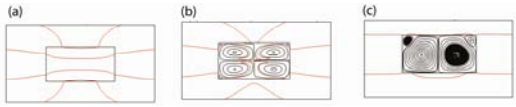

Figure 4: A close up view of the contour plot (in red) of temperature in the whole domain (rock and cavity) and streamline plot (in black) of velocity field in the cavity subdomain for cavity with as A=2, (a) only conductive heat transfer (Ra=0), (b) laminar convection (Ra=1E6), (c) turbulent convection (Ra=1E9)

Heat flux passing through an insolated and buried cavity is proportional to the cavity aspect ratio (*A*) and buoyancy forcing, while for an infinitely wide cavity (*A* is very large), heat flux only depends on buoyancy forcing. For isolated and buried cavities, as a cavity aspect ratio is increased, there is more heat flux passing through it. This is shown in Figure 5.

Figure 5 compares the behavior for isolated and buried cavities with *Nu* vs *Ra*. *Nu* is a ratio of total heat flux passing through any two cavity

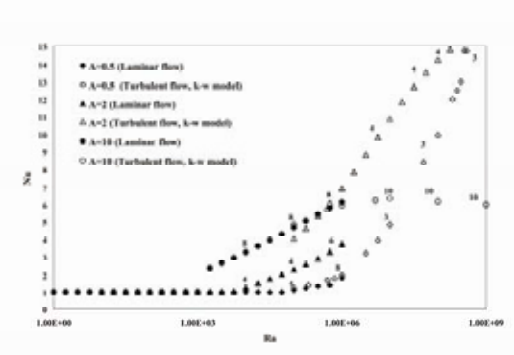

Figure 5: Comparison of *Nu* vs *Ra* behavior for isolated and buried cavities (numbers on the plot show number of convection cells at a particular *Ra*)

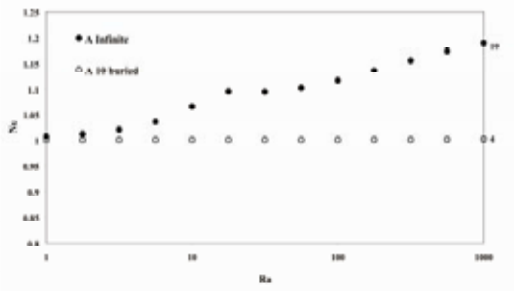

Figure 6: Comparison of *Nu* vs *Ra* behavior between isolated and buried cavity with A=10 and infinite cavity aspect ratio (numbers on the plot show number of convection cells at a particular *Ra*)

boundaries (one vertical and one horizontal) when there is conductive and convective heat transfer to heat flux passing through the same boundaries but when there is only conductive heat transfer.

Ra is a measure of buoyancy forcing Figure 6 compares *Nu* vs *Ra* behavior between an isolated cavity with *A*=10 and a cavity with an infinite aspect ratio. There is much more heat flux passing through an infinitely wide cavity with respect to an isolated and buried cavity because in the former case heat flux has no choice but to pass through the cavity, while in the latter case heat flux can by-pass the cavity and go around it.

Laminar and turbulent convection simulations show heat flux values, measured in terms of *Nu*, which are very close for an intermediate range of *Ra* (see Figure 5). This is because, for an intermediate range of *Ra* production of turbulent kinetic energy is very low and the specific dissipation rate of the turbulent kinetic energy is very high.

As cavity aspect ratio increases, the value of critical *Ra* (*Ra* at which convection starts) decreases. This inverse relationship is caused by "the rigid boundary effect" of the fixed side boundaries of the cavity. In cavities with a small aspect ratio, the fixed side boundaries have a stabilizing effect on the pattern of fluid flow by restricting convection motion.

The pattern of convection cells depends on both cavity aspect ratio and buoyancy forcing. For a cavity with *A*=10, we observed a single row of cells at an intermediate range of *Ra* (1E4 to 1E6) and when buoyancy forcing is increased in the cavity, convection cells become almost square. For cavities with *A* equals to either 0.5 or 2, we observed stacked cell formation (see Figure 4b) at an intermediate range of *Ra* (means laminar fluid flow), and some corner cells along with large cells, at the cavity center, for high *Ra*'s (means turbulent fluid flow). Also, as the buoyancy forcing is increased in a cavity with a fixed aspect ratio the mean fluid speed also increases.

Part 2:

Cavity slope affects the heat flux flow pattern in the surrounding rock mass in the proximity of the cavity, by encouraging heat flux to pass through the cavity rather than avoid it. This heat flux flow behavior is similar to the behavior reported for the cavity aspect ratio case.

For a sloping cavity and for a fixed cavity aspect ratio (*A*) and for a fixed applied heat flux (*q*), *Ra* exponentially increases with the effective length scale $H\cos(\theta)+L\sin(\theta)$, where H, θ, and L are the cavity height, the cavity slope from a horizontal line, and the cavity length, respectively. Note: H is the effective length scale for a horizontal cavity. For example, for a fixed q and A, if *Ra* is 1E5 for a horizontal cavity ($\theta=0^o$), corresponding *Ra* for a sloping cavity with $\theta=30^o$ is 2.54E9.

Convective heat transport is a preferred mechanism of heat transport in a sloping cavity. Figure 7 shows Nu vs Ra behavior for sloping cavities at a fixed Ra. In Figure (7), we have fixed *Ra* at 1E5 for laminar and at 1E7 for turbulent convection with varied cavity slopes indicating that simulated heat flux is lower for steeper cavity slopes. We tried to simulate laminar convection in a sloping cavity with a fixed q and a variable Ra using the model # 2 in

section # 2, which is good for higher Ra convection however, simulations yielded a convergence problem.

The pattern and number of cells in a sloping cavity are very sensitive to the cavity slope. The obtained *Nu* data for various cavity slopes indicates that a lesser number of convection cells encourage more convective heat transport with respect to conductive heat transport. Figure 7 shows the number of cells observed for each cavity slope with laminar and with turbulent convection at a fixed Ra. There exists a transition angle for laminar convection (between 53.75^o and 55^o cavity slope) for the laminar convection (at Ra=1E5), after which the pattern of cells does not change any further (see Figure 8 a, b). In contrast to this, for turbulent convection, for the converged simulations, we have not observed an angle with transition characteristics as high as 60^o.

Part 3:

Simulation results do not show any significant effects of a cavity shape on heat flow patterns in the surrounding rock mass in the proximity of a cavity with a fixed buoyancy forcing. Temperature contours in the proximity of the cavity have a similar pattern for all cavity shapes at a fixed Ra.

Large size cavities have more heat flux passing through them than small size cavities. This finding is consistent with the findings for heat flux flow pattern for a cavity aspect ratio case with an exception for a keyhole shaped cavity, shown in Table 2, case number 3. In the latter case, we found the Nu value nearly equal to the corresponding value for large cavities. Table 2 shows *Nu* for each of the six cavity geometries shown in Figure 2. We found an anomalous behavior for a circular shaped cavity, because *Nu* is very close to 1 for such a very high value of *Ra* (1E6) and has multiple convection cells arranged in a seemingly random order.

Cavity shape substantially affects shape and pattern of cells in a cavity. We have observed a single row of cells for the following cavity shapes: the rectangular cavity, the rectangular cavity with rounded corners, and the elliptical cavity [see Figure 9b for streamline pattern in an elliptical shaped cavity], while cavities with the following shape: the circle, square, and keyhole, all favor stacked cell formation [see Figure 9a for streamline pattern in a keyhole shaped cavity]. In addition to this, elliptical cavity shows a maximum number of cells (see Figure 9b) as in comparison to all six members of its group.

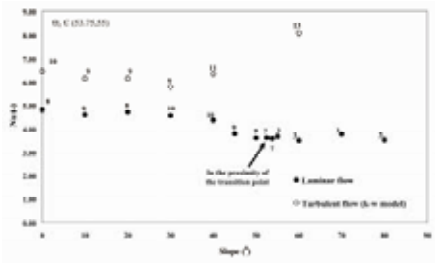

Figure 7: Variation of *Nu* wrt cavity slope at *Ra*=1E5 for laminar flow and at *Ra*=1E7 for turbulent flow (numbers on the plot show number of convection cells at a particular *Ra*)

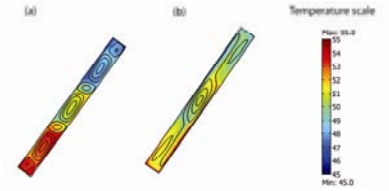

Figure 8: Surface plot of temperature and streamline plot of velocity field in a cavity with the slope of 53.75^o (a) and with the slope of 55^o (b) with a laminar fluid flow at Ra=1E5

Table 2: Comparison of *Nu* for cavities with various shapes with a laminar flow assumption at *Ra=1E6*

Cavity geometry	A	Nu	# of cells
circle	1	1.31	7
square	1	2.48	4
keyhole	1	5.30	3
rectangle	10	6.41	8
rectangle with rounded corners	10	6.77	9
ellipse	10	5.77	12

Figure 9: Streamline plot of velocity field for a keyhole shaped cavity (a) and for an elliptical shaped cavity (b) at *Ra*=1E6 with laminar flow assumption

The patter of cells in a keyhole shaped cavity is very different from the pattern showed by circular and square shaped cavity, which have a same aspect ratio as a keyhole shaped cavity. Thus, pattern of cells in a cavity is highly dependent on the relative closeness of the side boundaries (or cavity aspect ratio) and cavity shape.

4. Conclusions

In this work, we have numerically simulated laminar and turbulent natural convection in isolated and buried enclosures surrounded by a more conductive rock mass, as compared to an air-filled enclosure. Presence of a cavity affects pattern of the heat flux flow in the surrounding rock mass when there is only conductive heat flow in the surrounding rock mass and in the cavity. The heat flux generally avoids the cavity under this condition, which is caused by the insulation effect of the air-filled cavity. However, when buoyancy forcing in the cavity is increased, the insulation effect of an air-filled cavity decreases. This is because vigorously circulating air is more capable of transporting heat than stagnant air in a cavity. Critical *Ra*, at which convection onsets, has an inverse relationship with a cavity aspect ratio. Cavities with a small aspect ratio need more destabilizing forcing to onset convection, whereas, cavities with a large aspect ratio need relatively small destabilizing forcing for convection to start. Also, cavities with larger aspect ratios have more heat flux passing through them (larger *Nu*) as compared to cavities with smaller aspect ratios. Cavity aspect ratio along with buoyancy forcing plays an important role in governing number and pattern of convection cells in a cavity. Cavities with smaller aspect ratios prefer stacked cell formation for low to high *Ra* convection. Also, there are relatively small cells at the cavity corners for high *Ra* convection. Mean fluid speed increases and mean fluid temperature decreases in the cavity when buoyancy forcing is increased because high speed circulating fluid redistributes heat more efficiently.

Cavity slope has qualitatively similar effects on the heat flux pattern in the surrounding rock mass, in the proximity of a cavity, as a cavity aspect ratio has when buoyancy forcing is high. For a sloping cavity, convection heat transport is the preferred method for heat redistribution because *Nu* is large enough for a sloping cavity as in comparison to a horizontal cavity. In addition, there exists a transition angle for laminar convection after which the number of cells does not change any further in the cavity. However, based on numerical data, there is no such transition angle after which number of cells in the cavity does not change for turbulent flow convection at least up to 60^o cavity slope.

Based on the numerical data, cavity shape has no effect on heat flux pattern in the surrounding rock mass at a fixed buoyancy forcing. Cavity size and shape affect the pattern of cells. While circular, square, and keyhole shaped cavities (with A equals to 1) prefer stacked cell formation, cavities with a large (A=10) rectangular shape, rectangular with rounded corners, or elliptical shape prefer a single row of cells, the later resulting in a more efficient heat transport system. Convection cells, almost as if they were intelligent creatures, respond to cavity shape stimuli by arranging themselves in such a manner, which optimizes heat transfer for that cavity shape.

All the turbulent convection simulations reported in this paper is with high value of (isotropic) artificial diffusion, which is essential given the fact that our numerical formulation favors more convective fluxes of heat and momentum than diffusive fluxes of the same quantities. This is in addition to the fact that Galerkin Finite Element Method (used by COMSOL) is unstable for convection dominated problems ([8], [12]). Utilization of high artificial diffusion has subdued mean fluid speed and *Nu* for high *Ra* convection in a cavity. However, every attempt has been made to reduce the value of the tuning parameter for (isotropic) artificial diffusion parameter to as low a value as possible while still getting a converged simulation.

In the last, COMSOL Multiphysics software package is a useful numerical experimenting tool to understand convective flow and heat transport processes in enclosed environments. This statement is in the light of the fact that field experimentation technique for this purpose is very expansive and can not provide the in-depth behavior of various flow and heat transport parameters as numerical methods do.

8. References

[1] P. Le Quere, Onset of Unsteadiness, Routes to Chaos and Simulation of Chaotic Flows in Cavities Heated from the Side: A Review of Present Status, *Proceedings of the tenth International Heat Transfer Conference*, Bringhton, UK, 281-296 (1994).

[2] F. Ampofo and T. G. Karayiannis, Experimental benchmark data for turbulent natural convection in an air filled square cavity, *International Journal of Heat and Mass Transfer*, **46**, 3551-3572(2003).

[3] A. Bejan, Note on Grill's solution for free convection in a vertical enclosure, *J. Fluid Mech.*, 90, 561-568 (1979).

[4] A. Bejan, *Convection Heat Transfer*, John Wiley & Sons, Inc., 3rd edition (2004).

[5] D. R. Chenoweth and S. Paolucci, Natural convection in an enclosed vertical air layer with large horizontal temperature differences, *J. Fluid Mech.*, **169**, 173-210 (1986).

[6] R. Dwivedi, Modeling and field study of cave micrometeorology: Role of natural convection, Master's thesis, New Mexico Institute of Mining and Technology, Socorro, NM, USA, December (2009).

[7] D. J. Furbish, *Fluid Physics in Geology*, Oxford University Press, Inc., (1997).

[8] G. Hauke, A simple subgrid scale stablized method for the advection-diffusion-reaction equation, *Comput. Methods Appl. Mech. Engrg.*, **191**, 2925-2947(2002).

[9] J. Imberger, Natural convection in a shallow cavity with differentially heated end walls. Part 3. Experimental results. *J. Fluid Mech.*, **65**, 247-260 (1974).

[10] N. Z. Ince and B. E. Launder, On the computation of buoyancy-driven turbulent flows in rectangular enclosures. *Int. J. Heat and Fluid Flow*, **10**(2), 110-117 (1989).

[11] M. Jakob, *Heat Transfer*, John Wiley & Sons Inc., **1**, 522-542 (1957).

[12] V. John and Knobloch P., On spurious oscillations at layers diminishing (SOLD) methods for convection-diffusion equations: Part i-a review, *Comput. Methods Appl. Mech. Engrg.*, **196**, 2197-2215(2007).

[13] W. M. Kays, Turbulent prandtl number-where are we? *Transaction of ASME Journal of Heat Transfer*, **116**, 284-295 (1994).

[14] S. Kimura and A. Bejan, The boundary layer natural convection regime in a rectangular cavity with uniform heat flux from the side. *Transactions of ASME Journal of Heat Transfer*, **106**, 98-103 (1984).

[15] R. H. Kraichnan, Turbulent thermal convection at arbitrary prandtl number, *Physics of Fluids*, **5**(11), 1374-1389 (1962).

[16] R. Krishnamurti, On the transition to turbulent convection: Part 1, the transition from two- to three-dimensional flow, *J. Fluid Mech.*, **42**, 295-307 (1970).

[17] D. A. Nield and A. Bejan, *Convection in Porous Media*, Springer, 3rd edition (2006).

[18] S. Shindo, Micrometeorological modeling of an idealized cave and application to Carlsbad Cavern, NM, Master's thesis, New Mexico Institute of Mining and Technology, Socorro, NM, USA, December (2005).

9. Acknowledgements

We are very grateful to Dr. Mark Person, Dr. Rakhim Aitbayev, and COMSOL support team for helping us troubleshoot some of the modeling related problems. We are also very thankful to Dr. Julian Newmark, Belinda Harrison, and Katrina Koski for reviewing our manuscript.

10. Appendix

Table 3: Symbols and their interpretation

Symbol	Interpretation
L	Length of the domain (see figure 1a)
μ	Dynamic viscosity of fluid
K_f/K_r	ratio of thermal conductivities of fluid and rock (value 0.0102)
λ	Thermal diffusivity of fluid
T_1, T_2	Any dimensional temperature at computational domain's boundaries
H	Height of the domain (see figure 1a)
A	Aspect ratio (=L/H)
u, v	x- and y- components of dimensionless velocity field
T	Dimensionless temperature
Pr	Prandtl number of fluid
Ra	Rayleigh number $(=\frac{g\alpha q H^4}{\nu\lambda K_r})$
q_{av}	Total heat flux (convection and conduction) passing through a combination of a horizontal and a side boundary of a cavity
q_c	Total heat flux (conduction only) passing through a combination of a horizontal and a side boundary of a cavity (same boundaries as for q_{av})
Nu	q_{av}/q_c
k	Turbulent kinetic energy
ω	Specific rate of dissipation of turbulent kinetic energy
K_T	Turbulent thermal conductivity
F_{v1}	A parameter whose value is 0 for laminar fluid flow and 1 for turbulent fluid flow
Q	External heat source/sink
Pr_T	Turbulent prandtl number (value 0.9 from [13])
α	Turbulence modeling constant (value 13/25)
β_0	Closure coefficient in k-ω turbulence model (value 0.09)
σ_k	Turbulence modeling constant (value 0.5)
σ_{ω}	Closure coefficient (value 0.5)
β	Closure coefficient (value 9/125)
h	Local mesh element size
θ	Cavity slope from a horizontal line
g	Acceleration due to gravity
α	Volumetric thermal expansion coefficient for air
ν	Kinematic viscosity of air
q	Applied heat flux
$1E5$	10^5